Research Article

Samuel Dubuis, Paride Passelli* and Marco Picasso

Anisotropic Adaptive Finite Elements for an Elliptic Problem with Strongly Varying Diffusion Coefficient

https://doi.org/10.1515/cmam-2022-0036
Received February 8, 2022; revised April 7, 2022; accepted April 8, 2022

Abstract: The elliptic problem $-\operatorname{div}(\mu\nabla u) = f$ is considered, where $\mu > 0$ is smooth but strongly varying. Anisotropic a posteriori error estimates are derived, the effectivity index being bounded above and below by two constants independent of the data f, μ, the mesh size and aspect ratio, up to higher order terms. Numerical experiments on non-adapted and adapted anisotropic meshes confirm these predictions.

Keywords: A Posteriori Error Estimates, Adaptive Algorithm, Anisotropic Finite Elements, Elliptic Equation

MSC 2010: 65N30, 65N50

1 Introduction

Adaptive meshes have proved to be very efficient for solving PDEs at reduced computational cost given a prescribed level of accuracy. In the framework of finite elements methods, the adaptive criteria is often based on a posteriori error estimates, which were first derived for isotropic meshes [1, 7, 9, 16, 31, 36, 38] and more recently for anisotropic meshes [10, 11, 15, 19–21, 23, 26, 27, 30, 33, 34, 39], that is to say meshes with large aspect ratio. Anisotropic finite elements have demonstrated their efficiency when boundary or internal layers are involved, for instance in computational fluid dynamics [3, 4].

Here we focus on the elliptic problem $-\operatorname{div}(\mu\nabla u) = f$, where $\mu > 0$ is smooth but strongly varying. We will derive anisotropic a posteriori error estimates and show that the effectivity index (the ratio between the estimated error and the true error) is bounded above and below by two constants independent of the data f, μ, the mesh size and aspect ratio, up to higher order terms. These theoretical findings will be confirmed when using adapted meshes with large aspect ratio.

The outline of the paper is the following. In Section 2, we present the model equation and the numerical method. In Section 3, the anisotropic setting is introduced. In Section 4, we introduce the error estimator and state Theorem 1 which shows the equivalence between the true and the estimated error. In Section 5, numerical experiments with non-adapted meshes are performed. In Section 6, an adaptive algorithm is introduced, and its efficiency is demonstrated in both 2D and 3D situations. Finally, in Appendix A, the proof of Theorem 1 is presented.

***Corresponding author: Paride Passelli,** Institute of Mathematics, EPFL, 1015 Lausanne, Switzerland, e-mail: paride.passelli@epfl.ch
Samuel Dubuis, Marco Picasso, Institute of Mathematics, EPFL, 1015 Lausanne, Switzerland, e-mail: samuel.dubuis@epfl.ch, marco.picasso@epfl.ch. https://orcid.org/0000-0002-0069-5856

2 Problem Statement and Numerical Method

We consider a polygonal domain $\Omega \subset \mathbb{R}^2$ and a function $u : \Omega \to \mathbb{R}$ that is the solution of the elliptic equation

$$\begin{cases} -\operatorname{div}(\mu \nabla u) = f & \text{in } \Omega, \\ u = 0 & \text{on } \partial\Omega. \end{cases} \tag{2.1}$$

Throughout this paper, it is assumed that $f \in L^2(\Omega)$ and $\mu \in L^\infty(\Omega)$ such that there exist $\mu_{\min}, \mu_{\max}$ such that

$$0 < \mu_{\min} \leq \mu(x) \leq \mu_{\max}, \quad \text{a.e. } x \in \Omega.$$

Under these assumptions, there exists a unique weak solution $u \in H_0^1(\Omega)$ of (2.1). Moreover, if $\mu \in W^{1,\infty}(\Omega)$ and Ω is convex, then $u \in H^2(\Omega)$; see [22].

For any $h > 0$, let $\mathcal{T}_h$ be a conformal triangulation of Ω into triangles K of diameter $h_K \leq h$. Let V_h be the usual finite element space of continuous, piecewise linear, functions on triangles of $\mathcal{T}_h$, with zero value on $\partial\Omega$. To approximate the solution of (2.1), we are looking for $u_h \in V_h$ such that

$$\int_\Omega \mu \nabla u_h \cdot \nabla v_h = \int_\Omega f v_h \quad \text{for all } v_h \in V_h. \tag{2.2}$$

We will introduce an error estimator $\sum_{K\in\mathcal{T}_h} \eta_K^2$ equivalent to the numerical error $u - u_h$, that is to say there exist two constants $\hat{C}_1, \hat{C}_2 > 0$ that are independent of the data μ, f, the mesh size and aspect ratio such that

$$\hat{C}_1 \int_\Omega \mu |\nabla(u - u_h)|^2 \leq \sum_{K\in\mathcal{T}_h} \eta_K^2 \leq \hat{C}_2 \int_\Omega \mu |\nabla(u - u_h)|^2 \tag{2.3}$$

up to higher order terms. It is important to note that (i) (2.3) can be proved provided some local error term is equidistributed in the direction of maximum and minimum stretching – see assumption (4.2) hereafter – which is one of the goals of our adaptive algorithm; (ii) the error estimator η_K involves the exact solution, but post-processing techniques can be used to obtain an accurate approximation; (iii) the notion of higher order terms will be addressed more precisely in Remark 2.

3 Anisotropic Estimates for Clément's Interpolant

In the standard finite element theory, interpolation estimates involve constants that may depend on the aspect ratio and thus yield a posteriori error estimates that are not useful when using anisotropic finite elements. Recently, interpolation estimates that are sharp for meshes with large aspect ratio have been derived. We briefly recall the theoretical framework developed in [20, 21, 29]; similar results can be found in [23]. It should be noted that the maximum angle condition discussed in [5, 6] is not required; see [20, Section 2.1] for details. For simplicity, the presentation is done in a two-dimensional framework; it can easily be extended to the three dimensions.

For any $K \in \mathcal{T}_h$, we denote by $T_K : \hat{K} \to K$ one of the affine transformations mapping the reference triangle $\hat{K}$ into K defined by $\mathbf{x} = T_K(\hat{\mathbf{x}}) = M_K\hat{\mathbf{x}} + \mathbf{t}_K$, where $M_K \in \mathbb{R}^{2\times 2}$ and $\mathbf{t}_K \in \mathbb{R}^2$. Since M_K is invertible, it admits a singular value decomposition $M_K = R_K^T \Lambda_K P_K$, where R_K and P_K are orthogonal matrices and

$$\Lambda_K = \begin{pmatrix} \lambda_{1,K} & 0 \\ 0 & \lambda_{2,K} \end{pmatrix}, \quad \lambda_{1,K} \geq \lambda_{2,K} > 0, \quad R_K = \begin{pmatrix} \mathbf{r}_{1,K}^T \\ \mathbf{r}_{2,K}^T \end{pmatrix}.$$

In the above notation, $\mathbf{r}_{1,K}, \mathbf{r}_{2,K}$ are the unit vectors corresponding to the directions of maximum and minimum stretching, respectively, and $\lambda_{1,K}, \lambda_{2,K}$ correspond to the amplitude of the maximum and minimum stretching. A geometrical interpretation is shown in Figure 1. Note that, since T_K is not uniquely defined, then neither $\lambda_{i,K}, \mathbf{r}_{i,K}$, $i = 1, 2$, are.

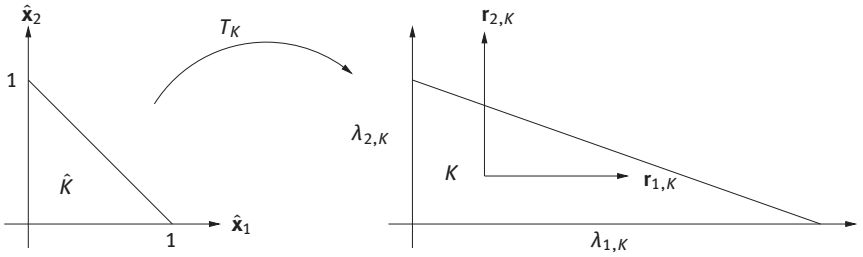

Figure 1: Transformation T_K mapping the usual reference element $\hat{K}$ into a right triangle K. The reference triangle is stretched in the direction $\mathbf{r}_{1,K} = (1, 0)^T$ (resp. $\mathbf{r}_{2,K} = (0, 1)^T$), with amplitude $\lambda_{1,K}$ (resp. $\lambda_{2,K}$).

Our goal is to derive residual-based, anisotropic a posteriori error estimates, the key ingredient being Clément's interpolant [14]. When using anisotropic meshes, some additional geometrical assumptions must be made in order to ensure that the constants involved in the interpolation estimates will not depend on the mesh aspect ratio. From now, it is assumed that

(1) for each K, the cardinality of ΔK, that is the union of triangles sharing a vertex with K, is uniformly bounded from above, independently of the mesh geometry,
(2) for each K, the diameter of $\Delta\hat{K} = T_K^{-1}(\Delta K)$ is uniformly bounded from above, independently of the mesh geometry.

In particular, the second assumption excludes too distorted meshes; see for instance [29]. It guarantees that all the quantities vary smoothly in the neighborhood of every triangle K. In practice, these assumptions are fulfilled when using available anisotropic mesh generators; see Section 6.

Let $R_h : H^1(\Omega) \to V_h$ be the Clément interpolant. Under the two above assumptions, the following interpolation error estimate can be proved.

Proposition 1 (Anisotropic Clément Interpolation Error Estimate [20, 21, 29, 34]). *There exists a constant $\hat{C} > 0$ depending only on the reference triangle $\hat{K}$, in particular independent of the mesh size and aspect ratio, such that, for any $v \in H^1(\Omega)$, for any $K \in \mathcal{T}_h$,*

$$\|v - R_h(v)\|_{L^2(K)} \le \hat{C}\omega_K(v), \tag{3.1}$$

and for any edge l_i, $i = 1, 2, 3$, of K,

$$\|v - R_h(v)\|_{L^2(l_i)} \le \hat{C}\Big(\frac{|l_i|}{\lambda_{1,K}\lambda_{2,K}}\Big)^{1/2}\omega_K(v), \tag{3.2}$$

where

$$\omega_K^2(v) = \lambda_{1,K}^2\|\nabla v \cdot \mathbf{r}_{1,K}\|_{L^2(\Delta K)}^2 + \lambda_{2,K}^2\|\nabla v \cdot \mathbf{r}_{2,K}\|_{L^2(\Delta K)}^2 = \lambda_{1,K}^2(\mathbf{r}_{1,K}^T G_K(v)\mathbf{r}_{1,K}) + \lambda_{2,K}^2(\mathbf{r}_{2,K}^T G_K(v)\mathbf{r}_{2,K}), \tag{3.3}$$

with

$$G_K(v) = \begin{pmatrix} \int_{\Delta K}\Big(\frac{\partial v}{\partial x_1}\Big)^2 & \int_{\Delta K}\frac{\partial v}{\partial x_1}\frac{\partial v}{\partial x_2} \\ \int_{\Delta K}\frac{\partial v}{\partial x_1}\frac{\partial v}{\partial x_2} & \int_{\Delta K}\Big(\frac{\partial v}{\partial x_2}\Big)^2 \end{pmatrix}.$$

4 The Anisotropic Error Estimator

We now introduce the error estimator. It is an improvement of the one presented in [34], adapted to the case of a non-constant diffusion coefficient μ. Letting $f \in L^2(\Omega)$, for all $K \in \mathcal{T}_h$, we define the $L^2(\Omega)$ projection of f onto the set of constant functions by

$$\Pi_K f = \frac{1}{|K|}\int_K f.$$

For a vector-valued function $\boldsymbol{f} = (f_1, f_2)$, we denote $\Pi_K \boldsymbol{f} =: (\Pi_K f_1, \Pi_K f_2)$, and for any edge l_i, $i = 1, 2, 3$, of K, we define

$$\Pi_{l_i} f = \frac{1}{|l_i|} \int_{l_i} f.$$

We then define the local error estimator η_K^2 by

$$\eta_K^2 = \left(\|\Pi_K f + \Pi_K \nabla\mu \cdot \nabla u_h\|_{L^2(K)} + \frac{1}{2} \sum_{i=1}^{3} \Big(\frac{|l_i|}{\lambda_{1,K}\lambda_{2,K}} \Big)^{1/2} \|[\Pi_{l_i} \mu \nabla u_h \cdot \boldsymbol{n}]\|_{L^2(l_i)} \right) \omega_K(u - u_h). \tag{4.1}$$

Here $\boldsymbol{n}$ stands for the unit outer normal to K, and ω_K is given by (3.3). For any edge l_i, $i = 1, 2, 3$, of K, we denote by $[\,\cdot\,]$ the jump across the edge l_i.

Observe that error estimator (4.1) is not standard since it involves the exact solution in the term $\omega_K(u - u_h)$ and thus is not fully computable. However, in practice, post-processing techniques can be applied in order to approximate the quantity $G_K(u - u_h)$, contained in $\omega_K(u - u_h)$, for instance Zienkiewicz–Zhu (ZZ) post-processing [2, 40, 41]. More precisely, we will replace

$$\frac{\partial(u - u_h)}{\partial x_i} \quad \text{by} \quad \Pi_h^{ZZ} \frac{\partial u_h}{\partial x_i} - \frac{\partial u_h}{\partial x_i}, \quad i = 1, 2,$$

where, for any $v_h \in V_h$, for any vertex P of the mesh,

$$\Pi_h^{ZZ} \frac{\partial v_h}{\partial x_i}(P) = \frac{\sum_{K \in \mathcal{T}_h, P \in K} |K| \frac{\partial v_{h|K}}{\partial x_i}}{\sum_{K \in \mathcal{T}_h, P \in K} |K|}$$

is an approximate $L^2(\Omega)$ projection of $\frac{\partial v_h}{\partial x_i}$ onto V_h.

It is well known [13, 41] that, for elliptic equations and structured meshes, superconvergence of the ZZ recovery occurs, implying that the post-processing is asymptotically exact, that is to say

$$\lim_{h \to 0} \frac{\|\Pi_h^{ZZ} \nabla u_h - \nabla u_h\|_{L^2(\Omega)}}{\|\nabla u - \nabla u_h\|_{L^2(\Omega)}} = 1.$$

On general meshes, it was first proven that $\|\Pi_h^{ZZ} \nabla u_h - \nabla u_h\|_{L^2(\Omega)}$ and the true error $\|\nabla u - \nabla u_h\|_{L^2(\Omega)}$ are equivalent; see for instance [24]. More recently, the superconvergence of the ZZ gradient recovery was finally shown for unstructured anisotropic meshes [12]. In general, the accuracy of the ZZ post-processing is better than the theoretical predictions, even on anisotropic meshes. We refer for instance to the numerical results presented in [11, 18, 27, 28, 32–35] in the case of anisotropic meshes for elliptic, parabolic and hyperbolic equations.

Under extra assumptions on f, μ and the mesh, it is possible to prove that the error estimator is equivalent to the true numerical error $u - u_h$, up to some higher order terms. The result is stated in the next theorem, whose proof is presented in Appendix A.

Theorem 1. *Assume that $f \in L^2(\Omega)$ and $\mu \in W^{1,\infty}(\Omega)$; let $u \in H_0^1(\Omega)$ be the weak solution of (2.1), and let $u_h \in V_h$ be the solution of (2.2). Moreover, assume that there exists $\hat{C} > 0$ depending only on the reference triangle $\hat{K}$ such that, for all $K \in \mathcal{T}_h$,*

$$\lambda_{1,K}^2 (\mathbf{r}_{1,K}^T G_K(u - u_h) \mathbf{r}_{1,K}) \le \hat{C} \lambda_{2,K}^2 (\mathbf{r}_{2,K}^T G_K(u - u_h) \mathbf{r}_{2,K}). \tag{4.2}$$

Then there exists a constant $\hat{C}_1 > 0$ depending only on the reference triangle such that

$$\int_\Omega \mu |\nabla(u - u_h)|^2 \le \hat{C}_1 \sum_{K \in \mathcal{T}_h} \Big(\eta_K^2 + \frac{\varepsilon_K^2}{\mu_{\min}} \Big),$$

where

$$\varepsilon_K^2 = \lambda_{2,K}^2 \Big(\|f - \Pi_K f\|_{L^2(K)}^2 + \|(\nabla\mu - \Pi_K \nabla\mu) \cdot \nabla u_h\|_{L^2(K)}^2 + \frac{1}{\lambda_{2,K}} \sum_{i=1}^{3} \|[(\mu - \Pi_{l_i}\mu) \nabla u_h \cdot \mathbf{n}]\|_{L^2(l_i)}^2 \Big).$$

Moreover, there exists a constant $\hat{C}_2 > 0$ depending only on the reference triangle $\hat{K}$ such that

$$\sum_{K \in \mathcal{T}_h} \eta_K^2 \le \hat{C}_2 \sum_{K \in \mathcal{T}_h} \Big(\int_K \mu |\nabla(u - u_h)|^2 \Big(1 + \frac{\|\mu - \Pi_K \mu\|_{L^\infty(\Delta K)}}{\mu_{\min}} \Big) + \frac{\varepsilon_K^2}{\mu_{\min}} \Big).$$

Remark 1. Assumption (4.2) means that the error in the maximal stretching direction is smaller than or equal to the error in the minimal stretching direction. This assumption was already used in [34] to derive the equivalence between the numerical error and the estimator. One possibility to fulfill (4.2) is to equidistribute for all $K \in \mathcal{T}_h$ the error in each direction $\mathbf{r}_{1,K}, \mathbf{r}_{2,K}$,

$$\lambda_{1,K}^2(\mathbf{r}_{1,K}^T G_K(u-u_h)\mathbf{r}_{1,K}) = \lambda_{2,K}^2(\mathbf{r}_{2,K}^T G_K(u-u_h)\mathbf{r}_{2,K}). \tag{4.3}$$

This requirement corresponds to the matching assumption discussed in [23]. Building a mesh such that (4.3) is satisfied will be ensured by the adaptive algorithm presented in Section 6. The algorithm has also the goal to align directions $\mathbf{r}_{1,K}, \mathbf{r}_{2,K}$ with respect to the eigenvectors of $G_K(u-u_h)$.

Remark 2. Assume $f \in H^1(\Omega)$ and $\mu \in W^{2,\infty}(\Omega)$. Then, from [20, 21], we have

$$\|f - \Pi_K f\|_{L^2(K)}^2 \leq \hat{C} \sum_{i=1}^{2} \lambda_{i,K}^2 \|\nabla f \cdot \mathbf{r}_{i,K}\|_{L^2(K)}^2.$$

Similarly, we have

$$\|(\nabla\mu - \Pi_K \nabla\mu)\cdot\nabla u_h\|_{L^2(K)}^2 \leq \hat{C}\left(\sum_{i,j=1}^{2} \frac{\lambda_{i,K}\lambda_{j,K}}{\lambda_{2,K}} \|\mathbf{r}_{i,K}^T H(\mu)\mathbf{r}_{j,K}\|_{L^\infty(K)}\right)^2 \|\nabla u_h\|_{L^2(K)}^2,$$

where $H(\cdot)$ denotes the Hessian matrix,

$$\sum_{i=1}^{3} \|[(\mu - \Pi_{l_i}\mu)\nabla u_h \cdot \mathbf{n}]\|_{L^2(l_i)}^2 \leq \hat{C}\left(\sum_{i=1}^{2} \lambda_{i,K}^2 \|\nabla\mu\cdot\mathbf{r}_{i,K}\|_{L^\infty(\partial K)}^2\right)\|\nabla u_h\cdot\mathbf{n}\|_{L^2(\partial K)}^2,$$

$$\|\mu - \Pi_K\mu\|_{L^\infty(K)} \leq \hat{C}(\lambda_{1,K}\|\nabla\mu\cdot\mathbf{r}_{1,K}\|_{L^\infty(K)} + \lambda_{2,K}\|\nabla\mu\cdot\mathbf{r}_{2,K}\|_{L^\infty(K)}).$$

In the isotropic framework, this yields a contribution

$$\sum_{K\in\mathcal{T}_h} \varepsilon_K^2 = O(h^3), \quad \text{which is negligible compared to} \quad \int_\Omega \mu|\nabla(u-u_h)|^2 = O(h^2).$$

In the anisotropic setting, for instance if f and μ depend only on x_2 and $r_{1,K} = (1,0)$, then $\varepsilon_K^2 = O(\lambda_{2,K}^3)$. Thus, in both cases, Theorem 1 indeed yields (2.3) up to higher order terms.

5 Numerical Experiments with Non-adapted Meshes

The goal of this section is to numerically verify the equivalence between the true error and the error estimator derived in Section 4. To this end, we consider problems with a known exact solution, and we define the following quantities: the error in H^1 seminorm

$$e_{H^1} = \|\nabla(u-u_h)\|_{L^2(\Omega)},$$

the error in the weighted H^1 seminorm

$$e_{\mu,H^1} = \|\mu^{1/2}\nabla(u-u_h)\|_{L^2(\Omega)},$$

the anisotropic estimator

$$\eta^A = \Big(\sum_{K\in\mathcal{T}_h} \eta_K^2\Big)^{1/2},$$

the anisotropic effectivity index

$$\mathrm{ei}^A = \frac{\eta^A}{e_{\mu,H^1}},$$

and the ZZ effectivity index

$$\mathrm{ei}^{ZZ} = \frac{\|\nabla u_h - \Pi_h^{ZZ}\nabla u_h\|_{L^2(\Omega)}}{e_{H^1}}.$$

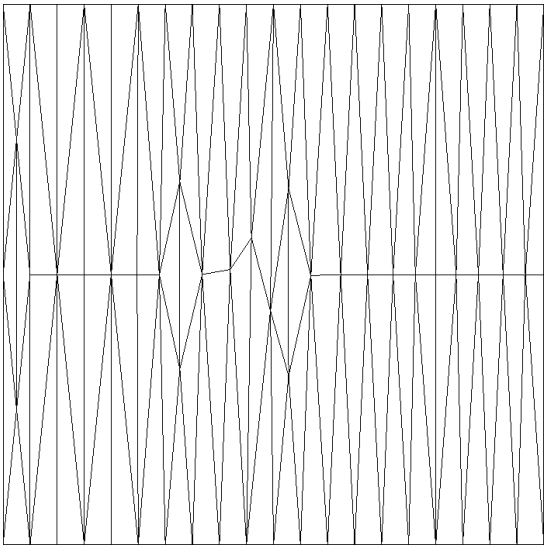

Figure 2: Example of non-adapted mesh with $h_1 = 0.05$ and $h_2 = 0.5$.

These quantities should satisfy the following properties:

- ei^A independent of the solution u,
- ei^A independent of the variations of μ and of the ratio $\frac{\mu_{\max}}{\mu_{\min}}$,
- ei^A independent of the mesh size and aspect ratio,
- ei^{ZZ} close to one.

For all $x \in \mathbb{R}$, $\epsilon > 0$, let

$$H_\epsilon(x) = \begin{cases} 0 & x \le -\epsilon, \\ \dfrac{x+\epsilon}{2\epsilon} + \frac{1}{2\pi}\sin\left(\dfrac{\pi x}{\epsilon}\right) & -\epsilon \le x \le \epsilon, \\ 1 & \epsilon \le x, \end{cases}$$

be a smoothing of the classical Heavyside function. We consider problem (2.1) in the unit square $\Omega = (0, 1)^2$ and choose f so that u is given by

$$u(\mathbf{x}) = \mu_2 \sin(\pi x_1)\sin(\pi x_2) H_\epsilon(x_1 - 0.5) + \mu_1 \sin(\pi x_1)\sin(\pi x_2) H_\epsilon(0.5 - x_1). \tag{5.1}$$

and μ is given by

$$\mu(\mathbf{x}) = \mu_2 H_\epsilon(x_1 - 0.5) + \mu_1\big(1 - H_\epsilon(x_1 - 0.5)\big), \tag{5.2}$$

with $\mu_1, \mu_2 > 0$. Thus μ is constant except in a thin boundary layer of width ϵ where a strong gradient can be observed. The results are reported in Table 1 with unstructured non-adapted meshes of various size, where h_1 and h_2 denote the mesh size in direction x_1 and x_2, respectively; see Figure 2. We observe that the error estimator is equivalent to the true error uniformly in the mesh size, the mesh aspect ratio and the ratio $\frac{\mu_{\max}}{\mu_{\min}}$. Moreover, the values of ei^{ZZ} show that the Zienkiewicz–Zhu error estimator is asymptotically exact.

6 An Adaptive Algorithm

We present an adaptive algorithm similar to the one presented in [33, 34]. For the sake of simplicity, we present the two-dimensional version of the algorithm, which can be easily extended to the three-dimensional case.

In all numerical experiments described hereafter, we observe that the anisotropic effectivity index converges to a number close to 3.45 as h goes to zero. In order to keep the effectivity index close to one, we will divide η_K by 3.45. To keep the notation simple, we still write η_K instead of $\eta_K/3.45$ in the sequel.

h_1-h_2	η^A	e_{μ,H^1}	ei^A	η^{ZZ}	e_{H^1}	ei^{ZZ}
			$\mu_1 = 1, \mu_2 = 2, \epsilon = 0.1$			
0.05-0.5	9.33	3.25	2.87	1.98	2.54	0.78
0.025-0.25	6.73	2.15	3.13	1.49	1.64	0.91
0.0125-0.125	3.96	1.38	2.87	0.99	1.05	0.95
0.00625-0.0625	2.10	0.73	2.87	0.53	0.55	0.97
0.003125-0.03125	1.07	0.36	2.93	0.27	0.28	0.98
0.0015625-0.015625	0.54	0.19	2.93	0.14	0.14	0.98
0.00078125-0.0078125	0.27	0.095	2.89	0.07	0.07	0.98
			$\mu_1 = 1, \mu_2 = 2, \epsilon = 0.01$			
0.05-0.5	91.07	36.24	2.51	20.67	29.83	0.69
0.025-0.25	63.39	23.47	2.70	14.44	19.72	0.73
0.0125-0.125	14.20	6.62	2.15	3.50	5.36	0.65
0.00625-0.0625	6.74	2.20	3.07	2.03	1.77	1.15
0.003125-0.03125	3.27	0.99	3.29	0.87	0.81	1.07
0.0015625-0.015625	1.67	0.51	3.28	0.42	0.42	1.02
0.00078125-0.0078125	0.85	0.26	3.30	0.21	0.21	1.00
			$\mu_1 = 1, \mu_2 = 100, \epsilon = 0.1$			
0.05-0.5	3584.94	1077.18	3.33	123.56	135.07	0.91
0.025-0.25	2395.20	764.94	3.13	85.30	89.35	0.95
0.0125-0.125	1365.70	469.50	2.91	50.27	52.43	0.95
0.00625-0.0625	715.23	246.22	2.90	26.23	26.89	0.98
0.003125-0.03125	359.39	120.49	2.98	12.94	13.13	0.99
0.0015625-0.015625	182.26	61.13	2.98	6.54	6.63	0.99
0.00078125-0.0078125	92.05	31.22	2.95	3.32	3.37	0.99
			$\mu_1 = 1, \mu_2 = 100, \epsilon = 0.01$			
0.005-0.05	3258.10	1183.14	2.75	162.95	183.48	0.89
0.0025-0.025	1517.05	450.98	3.36	66.70	65.89	1.01
0.00125-0.0125	777.60	231.73	3.36	32.19	32.01	1.01
0.000625-0.00625	375.00	110.71	3.39	15.60	15.61	1.00
0.0006-0.006	360.27	106.08	3.40	14.87	14.90	1.00

Table 1: True error, estimated error and effectivity index for various non-adapted meshes and various choices of μ_1, μ_2 and ϵ, when u and μ are given by (5.1) and (5.2).

The goal of the adaptive algorithm is to build a sequence of meshes with possibly large aspect ratio such that the relative estimated error is close to a prescribed tolerance TOL, i.e.

$$0.75\,\mathrm{TOL} \le \left(\frac{\sum_{K\in\mathcal{T}_h} \eta_K^2}{\int_\Omega \mu(\mathbf{x})|\nabla u_h|^2\, d\mathbf{x}} \right)^{1/2} \le 1.25\,\mathrm{TOL}\,. \tag{6.1}$$

We use the mesh generator BL2D [25] which requires information at the vertices rather than at the triangles. We define the error indicator for each vertex P as

$$\eta_P^2 = \sum_{\substack{K\in\mathcal{T}_h \\ P\in K}} \eta_K^2 \quad \text{so that} \quad \sum_{P\in\mathcal{T}_h} \eta_P^2 = 3 \sum_{K\in\mathcal{T}_h} \eta_K^2,$$

and (6.1) can be replaced by

$$0.75\,\mathrm{TOL} \le \left(\frac{\sum_{P\in\mathcal{T}_h} \eta_P^2}{3\int_\Omega \mu(\mathbf{x})|\nabla u_h|^2\, d\mathbf{x}} \right)^{1/2} \le 1.25\,\mathrm{TOL}\,.$$

We then equidistribute η_P^2 on each vertex P by adjusting the mesh with the objective to satisfy

$$\frac{3}{N_v} 0.75^2\,\mathrm{TOL}^2 \int_\Omega \mu(\mathbf{x})|\nabla u_h|^2\, d\mathbf{x} \le \eta_P^2 \le \frac{3}{N_v} 1.25^2\,\mathrm{TOL}^2 \int_\Omega \mu(\mathbf{x})|\nabla u_h|^2\, d\mathbf{x},$$

where N_v is the number of vertices of $\mathcal{T}_h$. In order to satisfy (4.2), we want to equidistribute the error in the directions of minimum and maximum stretchings, and therefore modify the mesh with the goal to satisfy, for $i = 1, 2$,

$$\frac{3\sigma_P}{2N_v} 0.75^2 \, \mathrm{TOL}^2 \int_\Omega \mu(\mathbf{x}) |\nabla u_h|^2 \, d\mathbf{x} \leq \sum_{\substack{K \in \mathcal{T}_h \\ P \in K}} \eta_{i,K}^2 \leq \frac{3\sigma_P}{2N_v} 1.25^2 \, \mathrm{TOL}^2 \int_\Omega \mu(\mathbf{x}) |\nabla u_h|^2 \, d\mathbf{x}, \tag{6.2}$$

where

$$\eta_{i,K}^2 = \left(\|\Pi_K f + \Pi_K \nabla \mu \cdot \nabla u_h\|_{L^2(K)} + \frac{1}{2} \sum_{j=1}^{3} \left(\frac{|l_j|}{\lambda_{1,K} \lambda_{2,K}} \right)^{1/2} \|[\Pi_{l_j} \mu(\mathbf{x}) \nabla u_h \cdot \mathbf{n}]\|_{L^2(l_j)} \right) \lambda_{i,K}^2 \mathbf{r}_{i,K}^T G_K (u - u_h) \mathbf{r}_{i,K}$$

and

$$\sigma_P = \frac{\sum_{K \in \mathcal{T}_h, P \in K} (\eta_{1,K}^2 + \eta_{2,K}^2)}{\sum_{K \in \mathcal{T}_h, P \in K} (\eta_{1,K}^4 + \eta_{2,K}^4)^{1/2}},$$

which satisfies $\frac{1}{\sqrt{2}} \leq \sigma_P \leq 1$.

The mesh generator BL2D requires for each vertex P the local mesh sizes $h_{1,P}$, $h_{2,P}$ and the angle θ_P between the direction of maximum stretching and the horizontal axis. We align the directions of maximum and minimum stretching with the eigenvectors of the post-processed gradient

$$G_P = \sum_{\substack{K \in \mathcal{T}_h \\ P \in K}} G_K (u - u_h).$$

More precisely, we set θ_P as the angle between the horizontal axis and the eigenvector corresponding to the largest eigenvalue of G_P. Concerning the local mesh sizes $h_{1,P}$, $h_{2,P}$, values $\lambda_{i,P}$, $i = 1, 2$, are computed at the vertices

$$\lambda_{i,P} = \frac{\sum_{K \in \mathcal{T}_h, P \in K} \lambda_{i,K}}{\sum_{K \in \mathcal{T}_h, P \in K} 1}.$$

Then, if the two inequalities in (6.2) are satisfied, we set $h_{i,P} = \lambda_{i,P}$; if the left inequality in (6.2) is not satisfied, we set $h_{i,P} = 1.5\lambda_{i,P}$; if the right inequality is not satisfied, we set $h_{i,P} = \lambda_{i,P}/1.5$. Starting from an initial coarse mesh and a coarse value of TOL, a sequence of 40 adapted meshes is generated. Then TOL is divided by two, 40 adapted meshes are generated, and so on. The results are reported hereafter.

Consider again problem (2.1) in the unit square $\Omega = (0, 1)^2$, with exact solution

$$u(\mathbf{x}) = \mu_2 \sin(\pi x_1) H_\epsilon(x_1 - 0.5) + \mu_1 \sin(\pi x_1) H_\epsilon(0.5 - x_1) \tag{6.3}$$

and μ defined by (5.2). We consider $\mu_1 = 1$, $\mu_2 = 2$ and $\epsilon = 0.01$. Note that the exact solution is not zero on the boundary anymore; thus, in principle, an extra-term should be added in the error estimator. However, numerical results indicate that this is not needed. Moreover, since the solution is one-dimensional, the adapted meshes will have very large aspect ratio. In Table 2, the results are reported when running the adaptive algorithm starting with TOL = 0.1 and an initial 10×10 uniform mesh. We reported also the maximum aspect ratio $\mathrm{ar}_{\max} = \max_{K \in \mathcal{T}_h} \frac{\lambda_{1,K}}{\lambda_{2,K}}$, the average aspect ratio $\mathrm{ar}_{\mathrm{av}}$, the total CPU time $\mathrm{CPU}_{\mathrm{tot}}$ and the CPU time spent in the adaptation of the mesh $\mathrm{CPU}_{\mathrm{adapt}}$ (seconds, Intel Core 2.80 GHz). Numerical results show the

TOL	Vertices	ei^A	e_{H^1}	ei^{ZZ}	$\mathrm{ar}_{\max}$	$\mathrm{ar}_{\mathrm{av}}$	$\mathrm{CPU}_{\mathrm{tot}}$	$\mathrm{CPU}_{\mathrm{adapt}}$
0.1	119	0.89	0.43	1.01	1679	355	7	6
0.05	196	0.94	0.22	0.99	3971	769	12	10
0.025	355	0.92	0.11	1.00	6643	1693	17	15
0.0125	741	0.96	0.054	1.00	17847	3055	25	21
0.00625	1388	0.99	0.027	1.00	37973	6683	36	31
0.003125	2822	0.98	0.013	1.00	77257	13292	55	47

Table 2: True error, effectivity indices and aspect ratio for different values of the tolerance TOL, when u and μ are given by (6.3) and (5.2), with $\mu_1 = 1$, $\mu_2 = 2$ and $\epsilon = 0.01$.

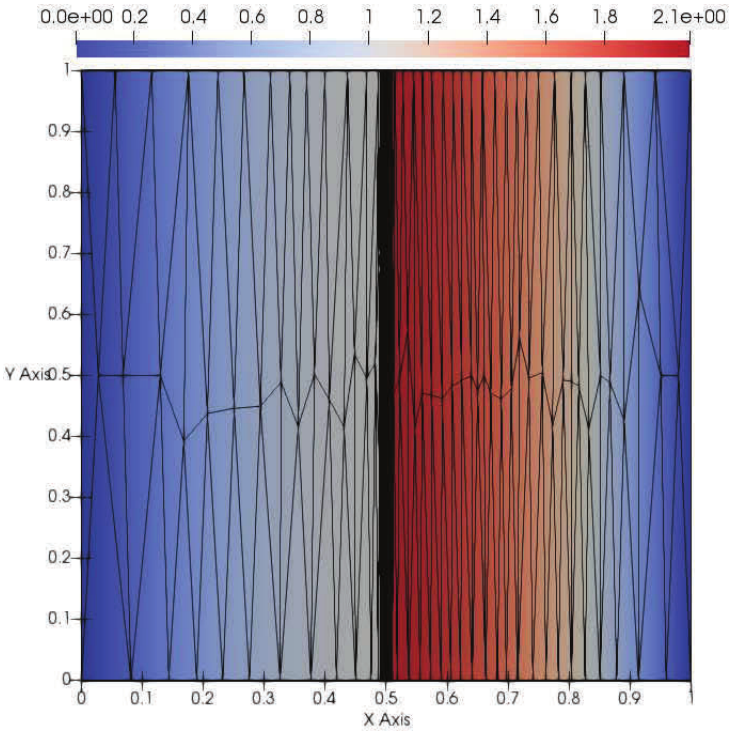

Figure 3: Solution on adapted mesh when TOL = 0.025, when u and μ are given by (6.3) and (5.2), with $\mu_1 = 1$, $\mu_2 = 2$ and $\epsilon = 0.01$.

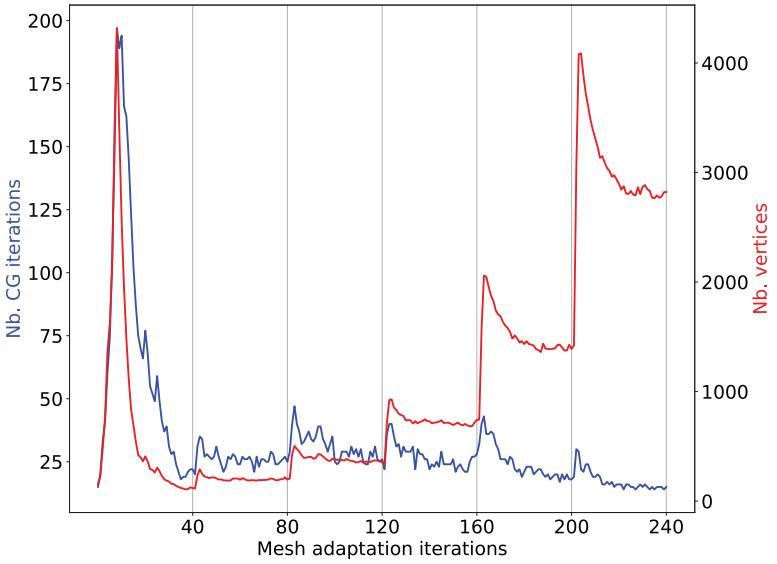

Figure 4: In blue: number of conjugate gradient iterations needed to reach a tolerance 10^{-8} for each iteration of the adaptive algorithm. In red: number of vertices of each adapted mesh at each iteration of the adaptive algorithm. The tolerance TOL is halved every 40 iterations of the adaptive algorithm.

sharpness of our anisotropic error indicator, although the mesh aspect ratio is very large. Moreover, most of the CPU time is spent for building adapted meshes rather than solving the linear systems. To illustrate this fact, the number of conjugate gradient iterations needed to solve the linear system together with the number of vertices are reported for all iterations of the adaptive algorithm in Figure 4. Each time the tolerance is halved, first the number of vertices increases and then decreases to a value which is twice the one obtained with the previous tolerance. This is due to the fact that vertices are first added in an isotropic manner and

TOL	Vertices	ei^A	e_{H^1}	ei^{ZZ}	ar_{max}	ar_{av}
			$\mu_1 = 1, \mu_2 = 2, \epsilon = 0.1$			
0.5	93	2.82	0.39	0.88	121	28
0.25	397	3.22	0.18	1.00	476	63
0.125	1525	3.28	0.09	1.00	589	99
0.0625	7511	3.27	0.05	0.99	1028	124
0.03125	39512	3.29	0.02	0.99	1769	166
			$\mu_1 = 1, \mu_2 = 2, \epsilon = 0.01$			
0.5	644	3.61	0.97	1.03	1220	173
0.25	2426	3.65	0.46	0.99	2533	257
0.125	13317	3.67	0.23	0.99	2552	277
0.0625	32479	3.56	0.12	0.98	12101	979
0.03125	214170	3.52	0.07	0.98	33075	1227
			$\mu_1 = 1, \mu_2 = 100, \epsilon = 0.1$			
0.5	107	3.42	32.62	0.99	234	45
0.25	366	3.45	15.67	1.03	377	72
0.125	1570	3.36	8.22	1.01	645	102
0.0625	7250	3.45	3.95	1.00	2024	132
0.03125	39129	3.44	1.96	0.99	1961	184

Table 3: True error, effectivity indices and aspect ratio for different values of tolerance TOL, when u and μ are given by (6.5) and (6.4), with various values for and μ_1, μ_2 and ϵ.

TOL	Vertices	ei^A	e_{H^1}	ei^{ZZ}	ar_{max}	ar_{av}	CPU_{tot}	CPU_{adapt}
0.25	191	1.06	195.85	1.01	864	143	23	19
0.125	452	1.09	85.17	1.04	4542	310	46	39
0.0625	1283	1.03	47.37	1.01	6684	694	94	78
0.03125	6426	1.01	26.36	0.99	15832	1098	292	237
0.015625	33745	1.10	13.60	0.99	117521	1588	2298	1402

Table 4: True error, effectivity indices and aspect ratio for different values of tolerance TOL, when u and μ are given by (6.5) and (6.4), with $\mu_1 = 1$, $\mu_2 = 100$ and $\epsilon = 0.01$.

then removed. Moreover, apart from the 40 first mesh iterations, the number of conjugate gradient iterations does not increase with the number of vertices due to the fact that, with mesh iterations, the initial guess of the conjugate gradient method is closer and closer to the solution of the linear system. In Figure 3, the mesh and solution obtained when TOL = 0.025 are shown.

We then present a 3D numerical experiment, the adaptive algorithm and the error estimator described above being adapted to the 3D case; see [17] for details. In order to produce adapted meshes, the 3D Precise Mesh software is used [42]. Letting $\Omega = (0, 1) \times (0, 1) \times (0, 0.1)$, we choose f such that μ is given by

$$\mu(\mathbf{x}) = \mu_2 H_\epsilon(x_3 - 0.05) + \mu_1(1 - H_\epsilon(x_3 - 0.05)) \tag{6.4}$$

and u by

$$u(\mathbf{x}) = \mu_2 \sin(\pi x_1) H_\epsilon(x_3 - 0.05) + \mu_1 \sin(\pi x_1) H_\epsilon(0.05 - x_3). \tag{6.5}$$

In Table 3, the results are reported when running the adaptive algorithm starting with an initial tolerance TOL = 0.5, an initial $10 \times 10 \times 2$ uniform mesh and several values of μ_1, μ_2 and ϵ. In Figures 5 and 6, the adapted mesh and solution are shown when TOL = 0.25 and $\mu_1 = 1$, $\mu_2 = 2$ and $\epsilon = 0.01$. Then, in order to keep the effectivity index close to one, η_K is divided by 3.45, and the adaptive algorithm is run again for several values of TOL when $\mu_1 = 1$, $\mu_2 = 100$ and $\epsilon = 0.01$. The results are reported in Table 4. As expected, the effectivity index is now close to one. Again, a non-negligible fraction of the CPU time is needed to adapt the mesh.

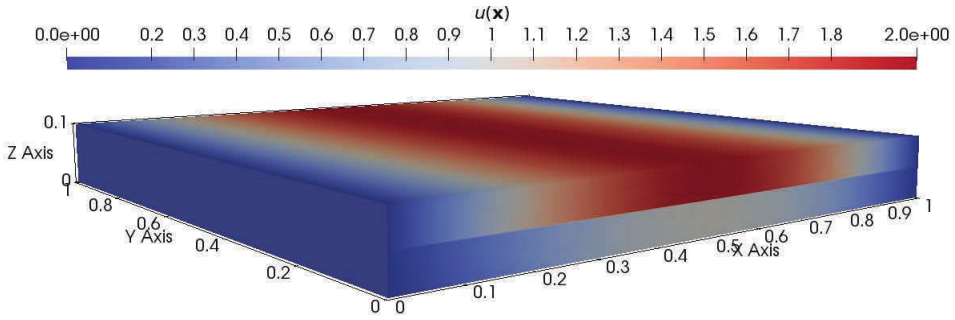

Figure 5: Solution on adapted mesh when TOL = 0.25, u and μ are given by (6.5) and (6.4), with $\mu_1 = 1$, $\mu_2 = 2$ and $\epsilon = 0.01$.

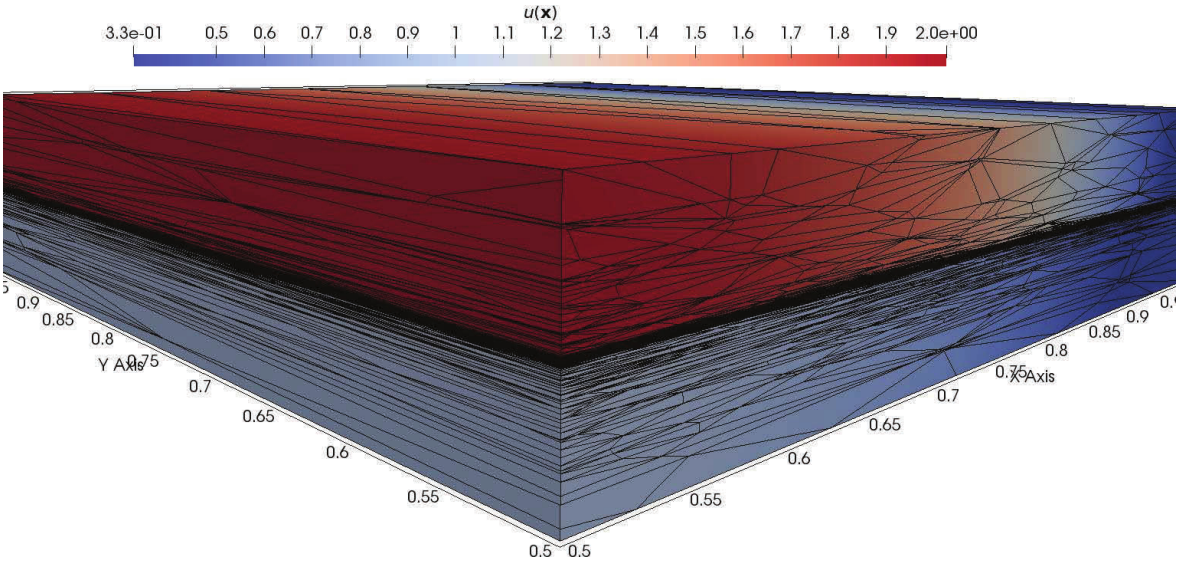

Figure 6: Cut at $x = 0.5$ and $y = 0.5$ of the adapted mesh obtained when TOL = 0.25, when u and μ are given by (6.5) and (6.4), with $\mu_1 = 1$, $\mu_2 = 2$ and $\epsilon = 0.01$.

7 Conclusion

We introduced an error estimator for the approximation of elliptic problems with strongly varying diffusion coefficient. The error estimator is shown to be equivalent to the true error, up to high order terms. An adaptive algorithm is presented, and its efficiency and accuracy is demonstrated with various numerical experiments.

A Appendix: Proof of Theorem 1

We first prove the upper bound. Letting $e = u - u_h$, using (2.1) and (2.2), we have, for any $v_h \in V_h$,

$$\int_\Omega \mu|\nabla e|^2 = \int_\Omega f(e - v_h) - \int_\Omega \mu \nabla u_h \cdot \nabla(e - v_h).$$

By integration by parts over the triangles K, we obtain

$$\int_\Omega \mu|\nabla e|^2 = \sum_{K\in\mathcal{T}_h} \int_K (f + \operatorname{div}(\mu\nabla u_h))(e - v_h) + \frac{1}{2}\int_{\partial K} [\mu\nabla u_h \cdot \boldsymbol{n}](e - v_h)$$

$$= \sum_{K\in\mathcal{T}_h}\int_K (\Pi_K f + \Pi_K\nabla\mu\cdot\nabla u_h)(e-v_h) + \frac{1}{2}\sum_{i=1}^{3}\int_{l_i}[\Pi_{l_i}\mu\nabla u_h\cdot\boldsymbol{n}](e-v_h)$$
$$+ \sum_{K\in\mathcal{T}_h}\int_K (f-\Pi_K f)(e-v_h) + \sum_{K\in\mathcal{T}_h}\int_K (\nabla\mu-\Pi_K\nabla\mu)\cdot\nabla u_h(e-v_h)$$
$$+ \frac{1}{2}\sum_{K\in\mathcal{T}_h}\sum_{i=1}^{3}\int_{l_i}[(\mu-\Pi_{l_i}\mu)\nabla u_h\cdot\boldsymbol{n}](e-v_h).$$

Using the Cauchy–Schwarz inequality, choosing $v_h = R_h e$ and by using interpolation error estimates (3.1) and (3.2), we obtain

$$\int_\Omega \mu|\nabla e|^2 \le \hat{C}\Bigg(\sum_{K\in\mathcal{T}_h}\eta_K^2 + \sum_{K\in\mathcal{T}_h}\Bigg(\|f-\Pi_K f\|_{L^2(K)} + \|(\nabla\mu-\Pi_K\nabla\mu)\cdot\nabla u_h\|_{L^2(K)} + \frac{1}{2\sqrt{\lambda_{2,K}}}\sum_{i=1}^{3}\|[(\mu-\Pi_{l_i}\mu)\nabla u_h\mathbf{n}]\|_{L^2(l_i)}\Bigg)\omega_K(e)\Bigg).$$

Using assumption (4.2) and the fact that $\mathbf{r}_{1,K}$, $\mathbf{r}_{2,K}$ form a basis, we have

$$\omega_K^2(e) \le \hat{C}\lambda_{2,K}^2(\mathbf{r}_{1,K}^T G_K(e)\mathbf{r}_{1,K} + \mathbf{r}_{2,K}^T G_K(e)\mathbf{r}_{2,K}) = \hat{C}\lambda_{2,K}^2\|\nabla e\|_{L^2(\Delta K)}^2.$$

We obtain the result by using the discrete Cauchy–Schwarz inequality.

In order to prove the lower bound, we use the standard bubble functions [8, 37], adapted to the anisotropic case in [34], and modified here to account for the variations of μ.

Proposition 2. *There exist a function $\varphi \in H_0^1(\Omega)$ and a constant $\hat{C} > 0$ (that depends only on the reference triangle $\hat{K}$) such that, for any $K \in \mathcal{T}_h$,*

$$\int_{l_i}[\Pi_{l_i}\mu\nabla u_h\cdot\boldsymbol{n}]\varphi = \left(\frac{|l_i|}{\lambda_{1,K}\lambda_{2,K}}\right)^{1/2}\|[\Pi_{l_i}\mu\nabla u_h\cdot\boldsymbol{n}]\|_{L^2(l_i)}\omega_K(e), \quad i=1,2,3, \tag{A.1}$$

$$\int_K(\Pi_K f + \Pi_K\nabla\mu\cdot\nabla u_h)\varphi = \|\Pi_K f + \Pi_K\nabla\mu\cdot\nabla u_h\|_{L^2(K)}\omega_K(e), \tag{A.2}$$

$$(\lambda_{1,K}^2\|\nabla\varphi\cdot\mathbf{r}_{1,K}\|_{L^2(K)}^2 + \lambda_{2,K}^2\|\nabla\varphi\cdot\mathbf{r}_{2,K}\|_{L^2(K)}^2)^{1/2} \le \hat{C}\omega_K(e), \tag{A.3}$$

$$\int_K \mu|\nabla\varphi|^2 \le \hat{C}(\Pi_K\mu + \|\mu-\Pi_K\mu\|_{L^\infty(K)})\frac{\omega_K^2(e)}{\lambda_{2,K}^2}. \tag{A.4}$$

Proof. We claim that

$$\varphi|_K = \hat{C}_K\Psi_K + \sum_{i=1}^{3}\hat{C}_{l_i}\Psi_{l_i},$$

where $\hat{C}_K$, $\hat{C}_{l_i}$ are constants that depend only on $\hat{K}$ and that have to be computed, and Ψ_K, Ψ_{l_i} are the usual bubble functions over K and its edges l_i, $i = 1, 2, 3$. For (A.1) and (A.2), the proof follows the same steps as the one of [34, Proposition 2]. In order to prove (A.3), we proceed again as in [34, Proposition 2] obtaining, for $i = 1, 2$,

$$\int_K|\nabla\varphi\cdot\mathbf{r}_{i,K}|^2 \le \hat{C}\frac{\omega_K^2(e)}{\lambda_{1,K}\lambda_{2,K}}\left(\int_K|\nabla\Psi_K\cdot\mathbf{r}_{i,K}|^2 + \sum_{j=1}^{3}\int_K|\nabla\Psi_{l_j}\cdot\mathbf{r}_{i,K}|^2\right),$$

which together with [21, relation (2.14)] gives (A.3). To prove (A.4), we note that

$$\int_K\mu|\nabla\varphi|^2 = \int_K\Pi_K\mu|\nabla\varphi|^2 + \int_K(\mu-\Pi_K\mu)|\nabla\varphi|^2$$

and then apply [34, Proposition 4]. □

We can now prove the lower bound. Using the definition of η_K^2 and identities (A.2) and (A.1), one can write

$$\sum_{K\in\mathcal{T}_h}\eta_K^2=\sum_{K\in\mathcal{T}_h}\int_K(\Pi_K f+\Pi_K\nabla\mu\cdot\nabla u_h)\varphi+\frac{1}{2}\sum_{i=1}^{3}\int_{l_i}[\Pi_{l_i}\mu\nabla u_h\cdot\boldsymbol{n}]\varphi,$$

where $\varphi\in H_0^1(\Omega)$ is the function given by Proposition 2. Therefore, adding and subtracting the correct quantities in the right-hand side, we have

$$\begin{aligned}\sum_{K\in\mathcal{T}_h}\eta_K^2=&\sum_{K\in\mathcal{T}_h}\int_K\mu\nabla e\cdot\nabla\varphi+\sum_{K\in\mathcal{T}_h}\int_K(\Pi_K f-f)\varphi+\sum_{K\in\mathcal{T}_h}\int_K(\Pi_K\nabla\mu-\nabla\mu)\cdot\nabla u_h\varphi\\&+\frac{1}{2}\sum_{K\in\mathcal{T}_h}\sum_{i=1}^{3}\int_{l_i}[(\Pi_{l_i}\mu-\mu)\nabla u_h\cdot\boldsymbol{n}]\varphi.\end{aligned}$$

Using the properties of the L^2 projection Π_K and Π_{l_i}, we obtain

$$\begin{aligned}\sum_{K\in\mathcal{T}_h}\eta_K^2=&\sum_{K\in\mathcal{T}_h}\int_K\mu\nabla e\cdot\nabla\varphi+\sum_{K\in\mathcal{T}_h}\int_K(\Pi_K f-f)(\varphi-\Pi_K\varphi)+\sum_{K\in\mathcal{T}_h}\int_K(\Pi_K\nabla\mu-\nabla\mu)\cdot\nabla u_h(\varphi-\Pi_K\varphi)\\&+\frac{1}{2}\sum_{K\in\mathcal{T}_h}\sum_{i=1}^{3}\int_{l_i}[(\Pi_{l_i}\mu-\mu)\nabla u_h\cdot\boldsymbol{n}](\varphi-\Pi_{l_i}\varphi).\end{aligned}$$

Integration by parts over the triangles $K\in\mathcal{T}_h$ and using the Cauchy–Schwarz inequality, we get

$$\begin{aligned}\sum_{K\in\mathcal{T}_h}\eta_K^2\le&\sum_{K\in\mathcal{T}_h}\|\mu^{1/2}\nabla e\|_{L^2(K)}\|\mu^{1/2}\nabla\varphi\|_{L^2(K)}\\&+\sum_{K\in\mathcal{T}_h}(\|(\Pi_K f-f)\|_{L^2(K)}+\|(\Pi_K\nabla\mu-\nabla\mu)\cdot\nabla u_h\|_{L^2(K)})\|\varphi-\Pi_K\varphi\|_{L^2(K)}\\&+\frac{1}{2}\sum_{K\in\mathcal{T}_h}\sum_{i=1}^{3}\|[(\Pi_{l_i}\mu-\mu)\nabla u_h\cdot\boldsymbol{n}]\|_{L^2(l_i)}\|\varphi-\Pi_{l_i}\varphi\|_{L^2(l_i)}.\end{aligned}$$

Now, using results from [20, 21], we have that there exists a constant $\hat{C}$ depending only on the reference triangle such that, for all K and all $i=1,2,3$,

$$\begin{aligned}\|\varphi-\Pi_K\varphi\|_{L^2(K)}&\le\hat{C}(\lambda_{1,K}^2\|\nabla\varphi\cdot\mathbf{r}_{1,K}\|_{L^2(K)}^2+\lambda_{2,K}^2\|\nabla\varphi\cdot\mathbf{r}_{2,K}\|_{L^2(K)}^2)^{1/2},\\\|\varphi-\Pi_K\varphi\|_{L^2(l_i)}&\le\frac{\hat{C}}{\sqrt{\lambda_{2,K}}}(\lambda_{1,K}^2\|\nabla\varphi\cdot\mathbf{r}_{1,K}\|_{L^2(K)}^2+\lambda_{2,K}^2\|\nabla\varphi\cdot\mathbf{r}_{2,K}\|_{L^2(K)}^2)^{1/2}.\end{aligned}$$

Finally, using the two bounds (A.3) and (A.4), Young's and the Cauchy–Schwarz inequalities, we obtain

$$\begin{aligned}\sum_{K\in\mathcal{T}_h}\eta_K^2\le\hat{C}\Bigg(&\int_\Omega\mu|\nabla e|^2+\sum_{K\in\mathcal{T}_h}(\Pi_K\mu+\|\mu-\Pi_K\mu\|_{L^\infty(K)})\frac{\omega_K^2(e)}{\lambda_{2,K}^2}\\&+\sum_{K\in\mathcal{T}_h}\Bigg(\|\Pi_K f-f\|_{L^2(K)}+\|(\nabla\mu-\Pi_K\nabla\mu)\cdot\nabla u_h\|_{L^2(K)}\\&+\frac{1}{2\sqrt{\lambda_{2,K}}}\sum_{i=1}^{3}\|[(\mu-\Pi_{l_i}\mu)\nabla u_h\cdot\boldsymbol{n}]\|_{L^2(l_i)}\Bigg)\omega_K(e)\Bigg).\end{aligned}\tag{A.5}$$

In order to conclude the proof, we note that

$$(\Pi_K\mu+\|\mu-\Pi_K\mu\|_{L^\infty(K)})\frac{\omega_K^2(e)}{\lambda_{2,K}^2}\le\hat{C}\|\mu^{1/2}\nabla e\|_{L^2(\Delta K)}^2+\hat{C}\frac{\|\mu-\Pi_K\mu\|_{L^\infty(\Delta K)}}{\mu_{\min}}\|\mu^{1/2}\nabla e\|_{L^2(\Delta K)}^2$$

The final result is obtained inserting the above estimate in (A.5).

Acknowledgment: The referees are acknowledged for fruitful suggestions.

Funding: Paride Passelli is financed by Rio Tinto Aluminium LRF Research Center at Saint Jean de Maurienne (EPFL industrial grant).

References

[1] M. Ainsworth and J. T. Oden, A posteriori error estimation in finite element analysis, *Comput. Methods Appl. Mech. Engrg.* **142** (1997), no. 1–2, 1–88.

[2] M. Ainsworth, J. Z. Zhu, A. W. Craig and O. C. Zienkiewicz, Analysis of the Zienkiewicz–Zhu a posteriori error estimator in the finite element method, *Internat. J. Numer. Methods Engrg.* **28** (1989), no. 9, 2161–2174.

[3] F. Alauzet, P. Frey and P. George, Anisotropic mesh adaptation for Rayleigh–Taylor instabilities, in: *ECCOMAS 2004 - European Congress on Computational Methods in Applied Sciences and Engineering*, University of Jyväskylä, Jyväskylä (2004), https://www.researchgate.net/publication/283138589.

[4] F. Alauzet and A. Loseille, A decade of progress on anisotropic mesh adaptation for computational fluid dynamics, *Comput.-Aided Des.* **72** (2016), 13–39.

[5] T. Apel, *Anisotropic Finite Elements: Local Estimates and Applications*, Adv. Numer. Math., B. G. Teubner, Stuttgart, 1999.

[6] I. Babuška and A. K. Aziz, On the angle condition in the finite element method, *SIAM J. Numer. Anal.* **13** (1976), no. 2, 214–226.

[7] I. Babuška, J. Chandra and J. E. Flaherty, *Adaptive Computational Methods for Partial Differential Equations*, Society for Industrial and Applied Mathematics, Philadelphia, 1983.

[8] I. Babuška, R. Durán and R. Rodríguez, Analysis of the efficiency of an a posteriori error estimator for linear triangular finite elements, *SIAM J. Numer. Anal.* **29** (1992), no. 4, 947–964.

[9] W. Bangerth and R. Rannacher, *Adaptive Finite Element Methods for Differential Equations*, Lectures in Math. ETH Zürich, Birkhäuser, Basel, 2003.

[10] E. Boey, Y. Bourgault and T. Giordano, Anisotropic space-time adaptation for reaction-diffusion problems, preprint (2017), https://arxiv.org/abs/1707.04787.

[11] Y. Bourgault and M. Picasso, Anisotropic error estimates and space adaptivity for a semidiscrete finite element approximation of the transient transport equation, *SIAM J. Sci. Comput.* **35** (2013), no. 2, A1192—A1211.

[12] W. Cao, Superconvergence analysis of the linear finite element method and a gradient recovery postprocessing on anisotropic meshes, *Math. Comp.* **84** (2015), no. 291, 89–117.

[13] C. Carstensen, All first-order averaging techniques for a posteriori finite element error control on unstructured grids are efficient and reliable, *Math. Comp.* **73** (2004), no. 247, 1153–1165.

[14] P. Clément, Approximation by finite element functions using local regularization, *Rev. Française Automat. Informat. Recherche Opérationnelle Sér.* **9** (1975), no. R2, 77–84.

[15] T. Coupez, Metric construction by length distribution tensor and edge based error for anisotropic adaptive meshing, *J. Comput. Phys.* **230** (2011), no. 7, 2391–2405.

[16] W. Dörfler, A convergent adaptive algorithm for Poisson's equation, *SIAM J. Numer. Anal.* **33** (1996), no. 3, 1106–1124.

[17] S. Dubuis, *Adaptive algorithms for two fluids flows with anisotropic finite elements and order two time discretizations*, Ph.D. thesis, Ecole polytechnique fédérale de Lausanne, 2019.

[18] S. Dubuis and M. Picasso, An adaptive algorithm for the time dependent transport equation with anisotropic finite elements and the Crank–Nicolson scheme, *J. Sci. Comput.* **75** (2018), no. 1, 350–375.

[19] L. Formaggia, S. Micheletti and S. Perotto, Anisotropic mesh adaption in computational fluid dynamics: Application to the advection-diffusion-reaction and the Stokes problems, *Appl. Numer. Math.* **51** (2004), no. 4, 511–533.

[20] L. Formaggia and S. Perotto, New anisotropic a priori error estimates, *Numer. Math.* **89** (2001), no. 4, 641–667.

[21] L. Formaggia and S. Perotto, Anisotropic error estimates for elliptic problems, *Numer. Math.* **94** (2003), no. 1, 67–92.

[22] P. Grisvard, *Elliptic Problems in Nonsmooth Domains*, Class. Appl. Math. 69, Society for Industrial and Applied Mathematics, Philadelphia, 2011.

[23] G. Kunert, An a posteriori residual error estimator for the finite element method on anisotropic tetrahedral meshes, *Numer. Math.* **86** (2000), no. 3, 471–490.

[24] G. Kunert and S. Nicaise, Zienkiewicz–Zhu error estimators on anisotropic tetrahedral and triangular finite element meshes, *M2AN Math. Model. Numer. Anal.* **37** (2003), no. 6, 1013–1043.

[25] P. Laug and H. Borouchaki, The BL2D mesh generator - beginner's guide, user's and programmer's manual, Technical report RT-0194, Institut National de Recherche en Informatique et Automatique (INRIA), Rocquencourt-Le Chesnay, 1996.

[26] A. Loseille and F. Alauzet, Continuous mesh framework part I: Well-posed continuous interpolation error, *SIAM J. Numer. Anal.* **49** (2011), no. 1, 38–60.

[27] A. Lozinski, M. Picasso and V. Prachittham, An anisotropic error estimator for the Crank–Nicolson method: application to a parabolic problem, *SIAM J. Sci. Comput.* **31** (2009), no. 4, 2757–2783.

[28] S. Micheletti and S. Perotto, Reliability and efficiency of an anisotropic Zienkiewicz–Zhu error estimator, *Comput. Methods Appl. Mech. Engrg.* **195** (2006), no. 9–12, 799–835.

[29] S. Micheletti, S. Perotto and M. Picasso, Stabilized finite elements on anisotropic meshes: A priori error estimates for the advection-diffusion and the Stokes problems, *SIAM J. Numer. Anal.* **41** (2003), no. 3, 1131–1162.

[30] J.-M. Mirebeau, Optimally adapted meshes for finite elements of arbitrary order and $W^{1,p}$ norms, *Numer. Math.* **120** (2012), no. 2, 271–305.

[31] M. Picasso, Adaptive finite elements for a linear parabolic problem, *Comput. Methods Appl. Mech. Engrg.* **167** (1998), no. 3–4, 223–237.
[32] M. Picasso, An anisotropic error indicator based on Zienkiewicz–Zhu error estimator: Application to elliptic and parabolic problems, *SIAM J. Sci. Comput.* **24** (2003), no. 4, 1328–1355.
[33] M. Picasso, Numerical study of the effectivity index for an anisotropic error indicator based on Zienkiewicz–Zhu error estimator, *Comm. Numer. Methods Engrg.* **19** (2003), no. 1, 13–23.
[34] M. Picasso, Adaptive finite elements with large aspect ratio based on an anisotropic error estimator involving first order derivatives, *Comput. Methods Appl. Mech. Engrg.* **196** (2006), no. 1–3, 14–23.
[35] M. Picasso, Numerical study of an anisotropic error estimator in the $L^2(H^1)$ norm for the finite element discretization of the wave equation, *SIAM J. Sci. Comput.* **32** (2010), no. 4, 2213–2234.
[36] R. Verfürth, A posteriori error estimation and adaptive mesh-refinement techniques, *J. Comput. Appl. Math.* **50** (1994), 67–83.
[37] R. Verfürth, *A Review of A Posteriori Error Estimation and Adaptive Mesh-Refinement Techniques*, Wiley-Teubner, New York, 1996.
[38] R. Verfürth, *A Posteriori Error Estimation Techniques for Finite Element Methods*, Oxford University, Oxford, 2013.
[39] J. Xu and Z. Zhang, Analysis of recovery type a posteriori error estimators for mildly structured grids, *Math. Comp.* **73** (2004), no. 247, 1139–1152.
[40] O. C. Zienkiewicz and J. Z. Zhu, A simple error estimator and adaptive procedure for practical engineering analysis, *Internat. J. Numer. Methods Engrg.* **24** (1987), no. 2, 337–357.
[41] O. C. Zienkiewicz and J. Z. Zhu, The superconvergent patch recovery and a posteriori error estimates. I. The recovery technique, *Internat. J. Numer. Methods Engrg.* **33** (1992), no. 7, 1331–1364.
[42] Spatial Corp Headquarters, Broomfield, 3D Precise Mesh, www.3ds.com.